J Solid State Electrochem (2009) 13:1645–1652
DOI 10.1007/s10008-009-0810-9

REVIEW

Electrochemical study on corrosion process characteristics of the high-strength low-alloy steels in $NaHSO_3$ solution

Weiming Liu · Yingqiao Zhang · Hanqian Zhang · Zhaoxia Qu · Jinfu Li

Received: 14 November 2008 / Revised: 16 February 2009 / Accepted: 18 February 2009 / Published online: 7 March 2009

Abstract Electrochemical methods were used to study the characteristics of corrosion process for the high-strength low-alloy steel and carbon steel used as a huge oil storage tank in $NaHSO_3$ solution. The polarization curve results show that both steel samples take place in active solution, and the high-strength low-alloy (HSLA) steel has higher i_{corr} value than carbon steel, which is due to the small grain size that provides high density of active sites for preferential attack. The electrochemical impedance spectroscopy (EIS) results make known that the corrosion process presents two stages. In the first 136 h, one-time constant in EIS diagrams can be shown. Both steels have similar corrosion resistance due to the combination effects of the grain size and microstructure. After 240 h of immersion, a complete passive film forms on the specimen surface, and two-time constants can be shown in EIS diagram. The HSLA steel exhibited improved corrosion resistance when compared with the carbon steel, which is due to the effect of the shape Fe_3C in microstructure and the deposition of $FeSO_4$ on the electrode surface. The scanning electrode microscopy analyses show that both steels take place in homogenous corrosion, and the carbon steel shows higher surface roughness and many Fe_3C residues. XRD results show that both steels have similar phase constitutes of corrosion products.

Keywords Electrochemical techniques · Electrochemical impedance spectra · Low-alloy steel · XRD

Introduction

The high-strength low-alloy (HSLA) steel is widely used as a huge oil storage tank in oil industry, which is often paid attention due to its excellent mechanical property and outstanding welding capability; however, the corrosion resistance of the HSLA steel is often overlooked. Therefore, the research about this aspect is very few. In fact, sulfurous substances seriously corrode the HSLA steel in a huge oil tank, which takes on two aspects: One is the sulfurous atmospheric corrosion. Many huge oil tanks are often built nearby the refinery, where the atmosphere contains a lot of SO_2, H_2S, etc., which have been seriously corroding the outer surface of the huge oil storage tank for a long time; the other is the sulfurous substance in the petroleum. The petroleum contains many inorganic and organic sulfurous compounds, for example, SO_2, H_2S, sulfite, sulfate, and so on, which have been eroding the inner surface of a huge oil tank for a long time. Therefore, it is highly essential to study the corrosion character and mechanism of the HSLA steel as a huge oil storage tank in sulfurous substance.

It is beneficial for the improvement of the corrosion resistance of the HSLA steel by increasing the content of alloy elements such as Cr, Mo, Cu, and Ni and suitable as a processing and heating technology and for the formation of steady-state passive film [1–3]. Generally, a passive film formed on the carbon steel can protect its surface from further corrosion, and electronic properties of passive film

Presented at the international conference CORROSION TODAY held in Gdansk-Sobieszewo, Poland, 23 to 26 April 2008

W. Liu (✉) · Y. Zhang · H. Zhang · J. Li
Shanghai Jiao Tong University,
Shanghai 200240, People's Republic of China
e-mail: liuweiming1979@gmail.com

H. Zhang · Z. Qu
Baosteel Research Institute,
Shanghai 200240, People's Republic of China

are expected to be of crucial importance in understanding their protective character against corrosion [4–6]. Since film dissolution, film formation, and breakdown involve the movement of the electrons and ions, electron properties represent one of the most significant features of a passive film with respects to its corrosion resistance [7].

Based on this, the purpose of this work was to investigate the corrosion character and mechanism of the HSLA steel in a huge oil tank. The electrochemical methods were employed, particularly the electrochemical impedance method. The steel passivating medium was $NaHSO_3$ solution of concentration 0.01 mol/L [8], in which $FeSO_4$ may form a protective film according to the following reactions:

$$Fe + H_2O \rightarrow Fe(OH)_2 + 2H^+ + 2e^- \quad (1)$$

$$Fe^{2+} + O_2 + SO_3^{2-} + H^+ \rightarrow FeSO_4 + H_2O \quad (2)$$

The second reaction is dependent on pH and the HSO_3^- concentration. Passivation of the HSLA steel occurs when the immersion time becomes sufficiently long, the formation of a γ-FeOOH/Fe_3O_4 film.

Experimental

Sample preparation

The material used for tests were the HSLA steel and common carbon steel in huge oil storage tank, in which compositions were shown in Table 1. The microstructure of the HSLA steel is bainite and that of the carbon steel is pearlite, as shown in Fig. 1. Every electrode specimen was a disc with a surface area of 1 cm^2, attached with a copper wire to its rear face. Every surface was embedded in epoxy resins, leaving the working surface of 1 cm^2. The polishing methods used to prepare for sample surface were as follows: First, the electrode surface was polished with emery paper (grade 400) and distilled water. The surface was then polished with emery paper (grade 600) until a homogeneous surface was obtained and then rinsed with acetone. Finally, the specimens were subjected for 5 min to ultrasonic washing with acetone. Electrochemical impedance spectroscopy (EIS) measurement began after an initial delay of 24 h for samples to reach a steady-state condition.

Experimental device descriptions

A typical three-electrochemical cell, consisting of a graphite bar counter electrode and a saturated calomel electrode (SCE) as reference electrode, was employed. Polarization curves and impedance experiments were registered with a VMP3 controlled by EC-lab software. For the potentiodynamic measurement, the sweeping potential is from –0.25 to 0.25 V with a scanning rate of 0.1667 mV/s. The impedance experiments were performed at free potential, applying a 5-mV amplitude sinusoidal signal in 10-kHz to 0.01-Hz frequency. The experimental data were analyzed by ZSimpWin software.

Surface characteristic

Scanning electrode microscopy (SEM) was utilized to investigate the corrosion scale morphology before and after the corrosion scale for the HSLA steel and carbon steel was removed. The microstructure of the corrosion scales was analyzed using X-ray diffractometer with filtered Cu Kα radiation.

Results and discussions

Surface character

The morphologies of corrosion scale were shown in Fig. 2. The rust layers of both specimens have an obvious delaminating phenomenon, namely an outer loose rust layer and an inner compact rust layer. The protective ability of corrosion products depends on the performance of the inner rust layer. Obviously, the corrosion product piled on the HSLA steel relatively compact on the electrode surface was shown in Fig. 2a, and an intact and loose corrosion scale on the carbon steel surface was shown in Fig. 2b. The compositions of the corrosion scale measured by XRD were shown in Fig. 3. It shows that the corrosion scale of specimens is all principally composed of the deposits ($FeSO_4.4H_2O$), corrosion products (α-FeOOH, γ-FeOOH, Fe_3O_4, Fe_2O_3), and residual cementite (Fe_3C).

Table 1 Chemical composition of the HSLA steel and the carbon steel (wt.%)

Specimen	Composition									
	C	Si	Al	Mo	Cr	Cu	Nb	Ni	S	P
HSLA steel	0.09	0.19	0.032	0.2	0.03	0.01	0.014	0.21	0.0015	0.0043
Carbon steel	0.14	0.30	0.034	–	0.02	–	0.017	0.02	0.004	0.012

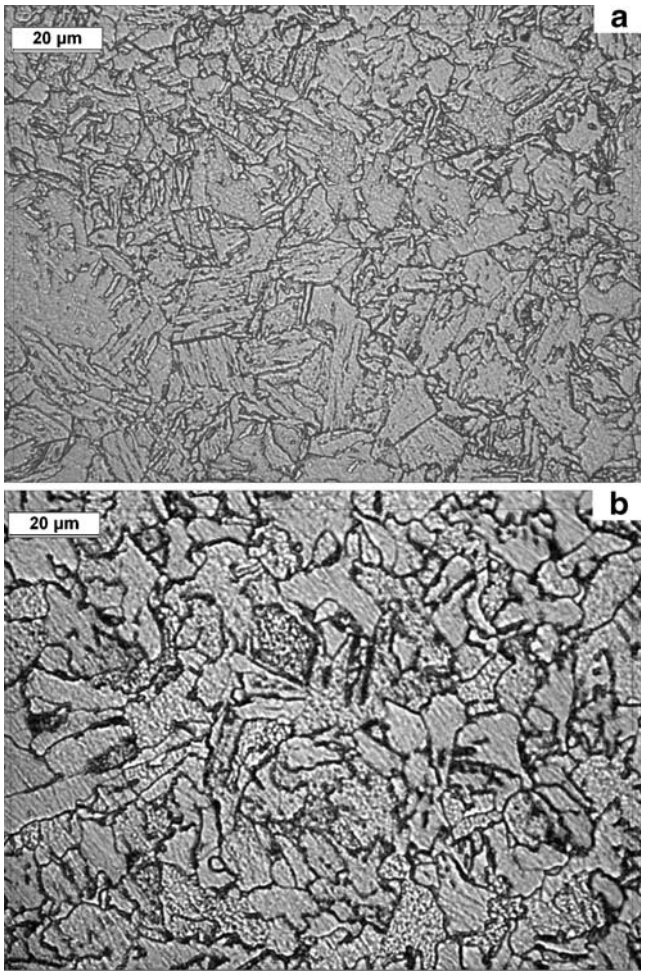

Fig. 1 Microstructure of samples: **a** HSLA steel and **b** carbon steel

Figure 4 shows SEM images of samples with corrosion scale removed after 572 h of immersion. It shows that both steels appear as a uniform corrosion. The carbon steel sample (Fig. 4b) shows a very rough surface and much Fe_3C remainders, indicating a serious corrosion in $NaHSO_3$ solution, while a flat surface morphology and few Fe_3C residues for the HSLA steel can be shown in Fig. 4a, which shows that it suffers light corrosion in $NaHSO_3$ solution.

Polarization measurements

Figure 5 shows potentiodynamic curves for both steels in $NaHSO_3$ solution. It shows that the anodic current density increases with increasing times, which demonstrates only active behavior and is unable to be passivated in the measured potential range. Table 2 shows that corrosion potentials (E_{corr}), polarization resistances (R_p), Tafel slopes (b_a and b_c, anodic and cathodic slopes, respectively), and corrosion currents (i_{corr}) were obtained from the polarization curves in $NaHSO_3$ solution. Generally, corrosion current density and corrosion potential are used to characterize the active dissolution ability of materials [9]. It can be shown that the corrosion current value of the HSLA steel is higher than that of the carbon steel, indicating that the corrosion rate of the HSLA steel is larger than that of the carbon steel, which is associated with the effects of the grain size and microstructure. It is well know that the grain boundaries are regions of preferable corrosion action because of the residual stress caused by plastic deformation in the boundaries during growth. As can be seen in Fig. 1, the HSLA steel has a small grain size, which has a higher number of activated sites and accelerates corrosion by forming much more microelectrochemical cells between the huge amount of grain boundaries and the matrix and by increasing the electrochemical reactivity during the corrosion process. Therefore, the HSLA steel has a higher corrosion rate in $NaHSO_3$ solutions.

Tafel slope values of potentiodynamic technique are considered the representative of corrosion process [10–12].

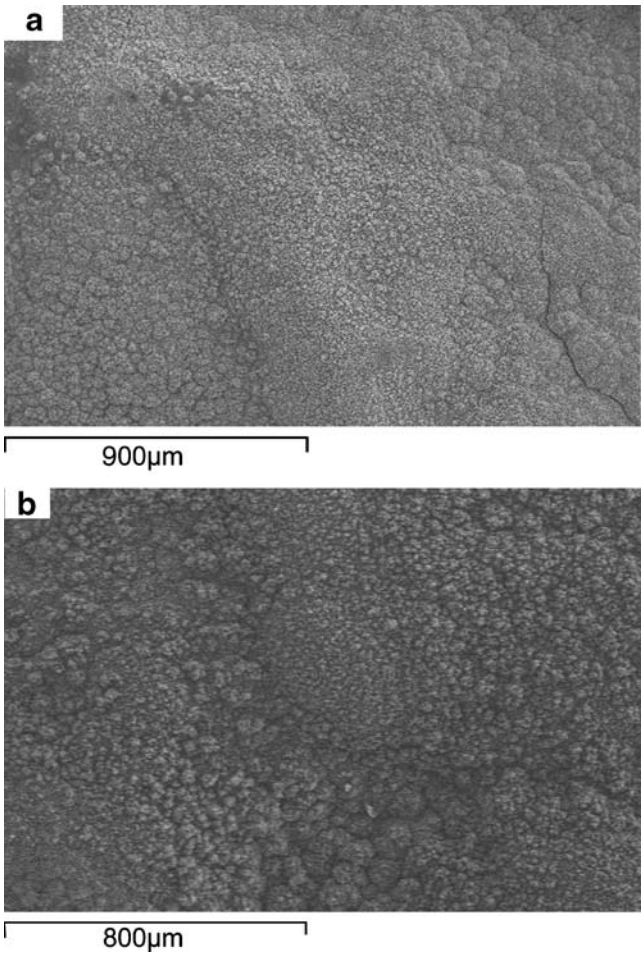

Fig. 2 SEM micrographs of corrosion scale: **a** HSLA steel and **b** carbon steel

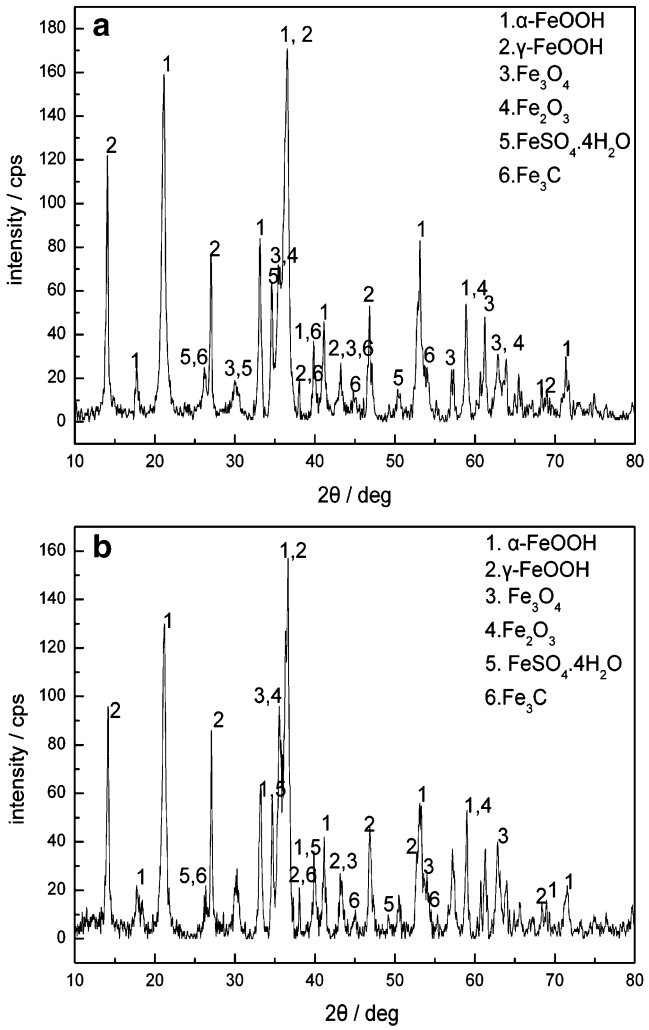

Fig. 3 X-ray diffraction of corrosion scale: **a** HSLA steel and **b** carbon steel

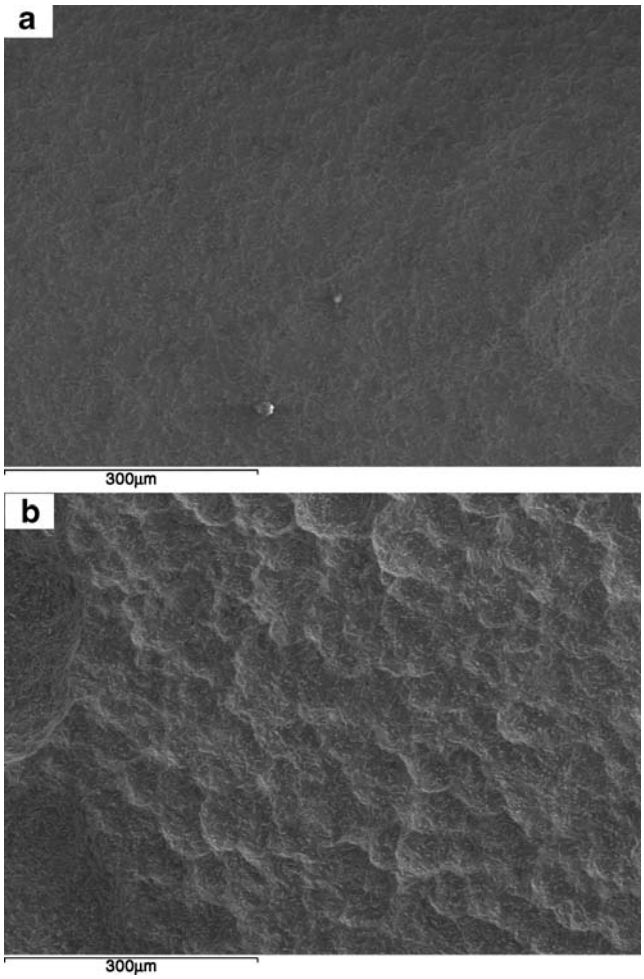

Fig. 4 SEM morphologies of removed scale: **a** HSLA steel and **b** carbon steel

Tafel slope value of cathode is greater than that of anode, which manifests the complex nature of the reduction process. The cathodic slope value of the HSLA steel is greater than that of the carbon steel, indicating that the cathodic reactions have been greatly affected by the grain size of specimens as mentioned above. These are also observed as the results of the corrosion current (i_{corr}).

EIS analysis of corrosion process

EIS has been widely used to study the electrical properties of the passive films formed on pure metals or alloys [13], whose electrical prosperities are expected to be of crucial importance in understanding their protective ability against corrosion. The working electrodes had been immersed in $NaHSO_3$ solutions until a stable rust layer formed. Figures 6 and 7 show the typical Nyquist diagrams and Bode diagrams obtained at the following times in $NaHSO_3$ solution: 48, 109, 128, 136, 240, 408 and 552 h. In these diagrams, different electrochemical behavior of the interface can be studied, and similar transformation processes are shown. At initial stage (before 136 h), the increased impedance arc upon immersion time is due to the deposit of

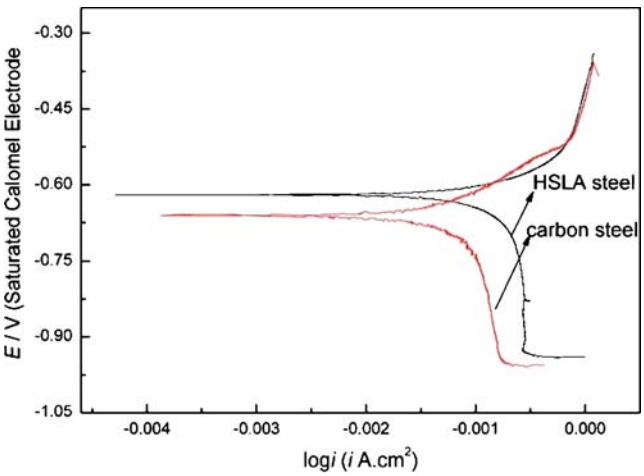

Fig. 5 Polarization curves obtained in $NaHSO_3$ solution

Table 2 Electrochemical parameters obtained from polarization curves

Sample	E_{corr} (V vs. SCE)	I_{corr} (A cm^{-2})	R_p (Ω cm^2)	β_a (V dec^{-1})	β_c (V dec^{-1})
HSLA steel	−0.62	1.53×10^{-4}	207.92	0.14	0.59
Carbon steel	−0.66	5.02×10^{-5}	562	0.14	0.27

corrosion product on the electrode. This indicates that the electrode was in an active dissolution state. However, the generated corrosion product and deposit were not sufficient to cover the whole surface of the electrode. As a result, one-time constant presents in EIS. With immersion time up to 240 h, the immersion time was so long that a layer of corrosion product covered over the electrode surface. Consequently, two-time constants are observed in Bode diagram. It can be seen that the diameter of the Nyquist plots is larger for the HSLA steel after 240 h of immersion, indicating the HSLA steel has better anti-corrosion ability in $NaHSO_3$ solution.

All experiment plots have a depressed semicircular shape in the complex impedance plane, with the center under the real axis; this behavior is typical for solid metal electrode that shows frequency dispersion of the impedance data [14]. Electrically equivalent circuit is generally used to model electrochemical behavior and to calculate the parameters of interest such as electrolyte resistance (R_s), charge transfer resistance (R_{ct}), and double-layer capacitance (C_{dl}) [15]. When a non-ideal frequency response is present, it is commonly accepted to distribute circuit elements. The most widely used is constant phase element (CPE), which has a non-integer power dependence on the frequency. Impedance is calculated by the expression:

$$Z_{CPE} = Y_0^{-1}(i\omega)^{-n}$$

Y_0 is the CPE admittance, $j=(-1)^{1/2}$, ω is the angular frequency of a disturb signal, n is the exponent of CPE

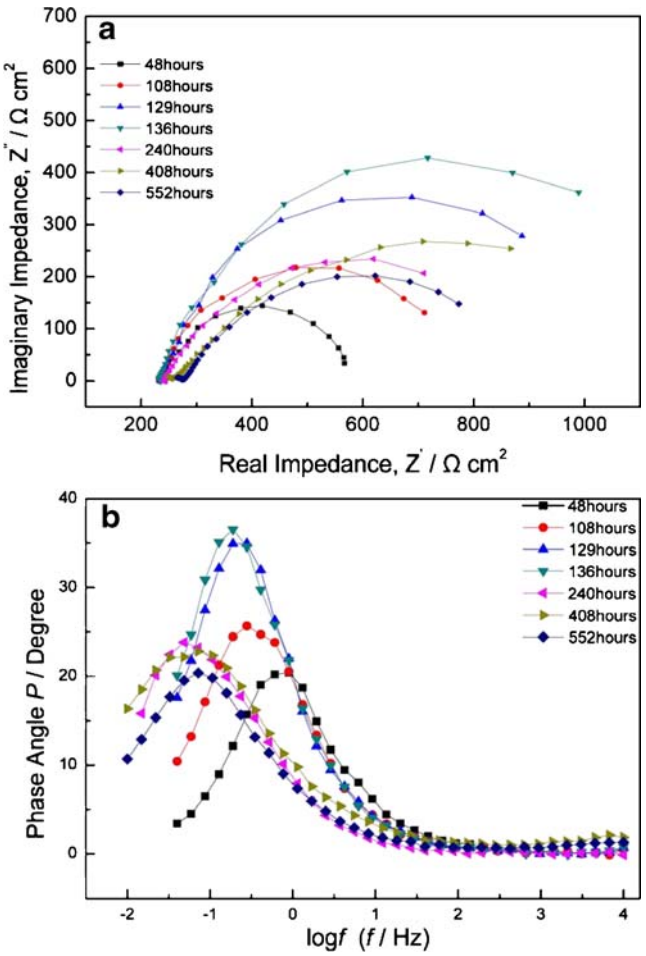

Fig. 6 Impedance spectra of HSLA steel in $NaHSO_3$ solutions: **a** Nyquist plots and **b** Bode plots

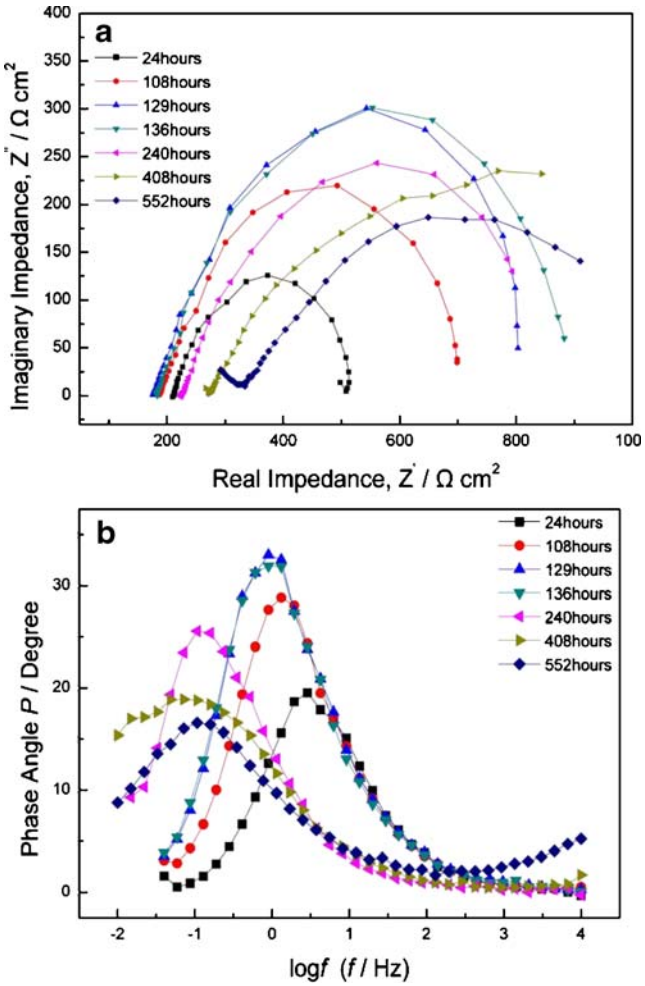

Fig. 7 Impedance spectra of carbon steel in $NaHSO_3$ solutions: **a** Nyquist plots and **b** Bode plots

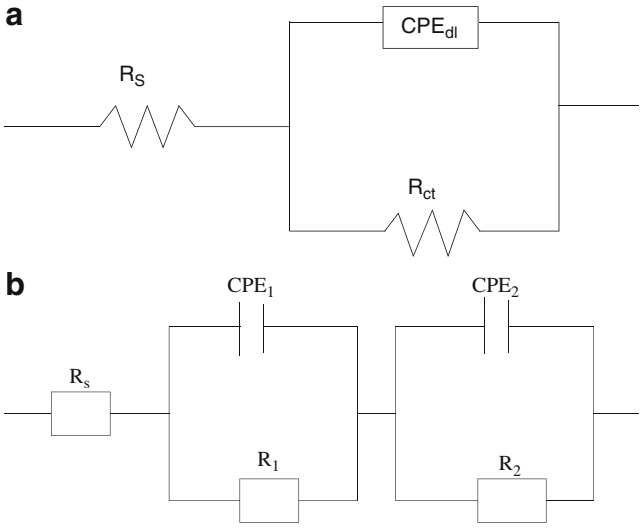

Fig. 8 **a** and **b** Equivalent circuits used to fit experimental data of EIS diagrams for HSLA steel in $NaHSO_3$ solutions

dispersion effect, and the scope of the n value is $0<n<1$. For example, a rough or porous surface can cause a double-layer capacitance to appear as a CPE with an n value between 0.9 and 1 [16]. An n value of 1 describes CPE as the pure capacitance; when an n value is equal to 0.5, CPE is a Warburg resistance; when an n value is equal to 1, CPE represents a pure capacitance [17].

The best agreements between experiment and fitting obtained with the equivalent circuits were illustrated in Fig. 8. Tables 3 and 4 show the representative parameter values of the best fit to experimental data in Figs. 6 and 7. In Fig. 8, R_s is the solution impedance, R_{ct} and R_f are the reaction resistance and film resistance, respectively, CPE_{dl} is constant phase element of the double layers, and CPE_f is constant phase element of corrosion film. Y_{dl} is admittance of CPE_{dl}, and n_{dl} is the exponent of CPE_{dl} dispersion effect. Tables 3 and 4 show the main parameters obtained with the equivalent circuits in Fig. 8. It can be seen that R_f values are superior to R_{dl} values, which indicates that the protection ability is mainly provided by the corrosion films.

The polarization resistance (R_p) is a typical resistance of overall electrode, which is associated with the corrosion current [18]. The R_p is equal to R_1 in the first 136 h and sum of R_1 and R_2 after 240 h of immersion. The R_p values obtained by analyzing impedance spectra were presented in Tables 3 and 4. R_p values generally increase with time first and then decreases. Both steels present an increase in R_p values at the beginning of the experiment, which indicates that the formation of a density and homogenous corrosion product can slow down the corrosion rate. After reaching certain exposure time (129–336 h), the increase of the reaction impedance of the HSLA steel is rather slow (696.6–744.9 Ω cm^2, respectively). It can be shown that the formation of the stable corrosion scale makes the H^+ diffuse difficult. The variation of R_p values of the carbon steel with time is more pronounced as well as presence of a maximum R_p value of about 998 Ω cm^2 at 408 h. The decreased R_p values for both steels are due to the department of some corrosion scales at the end of the experiment. Both steels show similar R_p values at the initial corrosion stage, which are the combination effects of the grain size and microstructure. The small grain size of the HSLA steel has higher corrosion rate and quickly forms corrosion products on the electrode, which can decrease the corrosion rate. In addition, the pearlite has a bad effect on the corrosion behavior on the steel [19, 20]. As a result, both steels have similar corrosion rate. The R_p values of the HSLA steel are much higher than those of the carbon steel at the end of experiment. It is because that the stable passive film completely covers with the samples surface, which can protect the sample surface from further corrosion. The HSLA steel can quickly form a continuous and protective passive film due to a small grain size, which increases the difficulty of H ions and electrons migrating to the surface to participate in further electrochemical reaction. In addition, the HSLA steel has the adhesion strength between the passive film and the reaction surface due to the increase in the electron activity at the grain boundary

Table 3 Equivalent circuit fitting for the HSLA steel in $NaHSO_3$ solution

Immersion time/h	R_s/Ω cm^2	Y_{dl}/Ω^{-1} cm^{-2} s^n	n_{dl}	R_{ct}/Ω cm^2	Y_f/Ω^{-1} cm^{-2} s^n	n_f	R_f/Ω cm^2	R_p/Ω cm^2
48	234.3	1.15×10^{-3}	0.80	353.4				353.4
109	232.8	1.18×10^{-3}	0.84	559				559
129	226.3	1.89×10^{-3}	0.87	857.7				857.7
136	235.9	1.80×10^{-3}	0.89	993.5				993.5
240	262	1.45×10^{-3}	1.00	509.5	5.56×10^{-3}	0.76	197.2	706.7
408	254.3	4.15×10^{-3}	0.65	949.4	2.88×10^{-4}	0.26	80.5	1029.9
552	280.8	5.73×10^{-3}	0.80	531.1	1.90×10^{-3}	0.37	103.3	634.4

Table 4 Equivalent circuit fitting for carbon steel in $NaHSO_3$ solution

Immersion time/h	$R_s/\Omega\ cm^2$	$Y_{dl}/\Omega^{-1}\ cm^{-2}\ s^n$	n_{dl}	$R_{ct}/\Omega\ cm^2$	$Y_f/\Omega^{-1}\ cm^{-2}\ s^n$	n_f	$R_f/\Omega\ cm^2$	$R_p/\Omega\ cm^2$
48	274	3.77×10^{-4}	0.81	352.3				352.3
109	190.9	5.36×10^{-4}	0.83	540.7				540.7
129	180.2	6.14×10^{-4}	0.80	696.6				696.6
136	186.3	6.36×10^{-4}	0.82	744.9				744.9
240	225	4.42×10^{-3}	0.65	171.2	5.48×10^{-3}	1.00	430.5	601.7
408	270	7.63×10^{-3}	0.98	214.2	3.43×10^{-3}	0.54	783.8	998
552	301	5.14×10^{-3}	0.24	96.4	3.23×10^{-3}	0.66	654.2	750.2

and possible pegging of the passivity film into grain boundaries [21, 22]. On the other hand, the size and shape of Fe_3C in microstructure affect the cathode reactions ratio, which would be discussed later.

The fitting results show that the proportional factor Y_{dl} of CPE_{dl} increases with time for both steels. According to Turgoose et al. [23], this increase in the capacitance Y_{dl} value is associated with an increase in double-layer capacitance due to an increase in the surface area available for cathodic reaction, which is related to the electrochemical activity of non-oxidized cementite (Fe_3C) residue exposed after the corrosion process. However, this would lead to a decrease in R_p values with time (higher corrosion rates), in contrast to the results obtained in this work, which present a rising tendency through time for these values. To explain this behavior, an important aspect of this process must be considered. When corrosion reactions take place, the area of Fe_3C exposure increases for the carbon steel. That is because the dissolution of the surrounding ferrite from the pearlite leaves a laminar structure of non-oxidized Fe_3C, as shown in Fig. 4b, which is not removed from the sample surface. In the case of the HSLA steel, of which microstructure is the bainite, the shape of Fe_3C is small. When the surrounding ferrite is dissolved, the small Fe_3C phase is easy to detach from the metal surface and leaves a few Fe_3C residues in the $NaHSO_3$ solution, which can be shown in Fig. 4a. Therefore, the cathodic areas remain steady for the HSLA steel. As a result, the increased capacitance values for the HSLA steel cannot be obviously affected by the increased area of the residual Fe_3C.

The $FeSO_4$ can deposit on the sample surface as shown in XRD result. As iron sulfate precipitate, they develop a surface layer over corrosion metal. These scales are porous and inhomogeneous, allowing the access of corrosion solution to the base metal. However, with the immersion time increasing, these scales can seem to cover over the electrode surface and provide good corrosion protection to the metal beneath them by restricting the mass transfer of reactants and products between the solution and metal [24]. Therefore, a second time constant in the EIS Bode plots can be seen in Figs. 6 and 7, which indicates that $FeSO_4$ films were forming on the sample surface. Consequently, an increase in the capacitance values could be related to the growing area of iron sulfate deposit over the surface of the samples, which is accompanied by an increase in the corresponding R_p values.

Based on the above analysis, the samples of the carbon steel had high thickness of corrosion scale at the end of the experiment, which was caused by higher corrosion rates and the deposit of $FeSO_4$ films. According to the Helmholtz model, $C_{dl} = \varepsilon_0 \varepsilon A/\delta$; thus, the Y_{dl} values for the HSLA steel are larger than those obtained for the carbon steel. ε is the dielectric constant of the medium, ε_0 is the vacuum permittivity, A is the electrode area, and δ is the thickness of the protective layer. The rising of n_{dl} factor agrees with this assumption because it can be attributed to an increase of the homogeneity resulting from the formation of deposit on the electrode surface.

Conclusions

1. The polarize curve results show that the HSLA steel has higher I_{corr} value than the carbon steel, and it indicates that the HSLA steel is prone to erode in $NaHSO_3$ solution. The rust layer of HSLA steel is more compact than that of carbon steel. Therefore, it has better protective ability. The rust layer of the HSLA steel and carbon steel similarly consist of $FeSO_4.4H_2O$, α-FeOOH, γ-FeOOH, Fe_3O_4, Fe_2O_3, and Fe_3C.
2. The electrochemical characteristic of HSLA steel and carbon steel was studied by the EIS diagram. Based on EIS diagrams with different times, it can be seen that they have similar corrosion process in $NaHSO_3$ solution. Both steels have similar corrosion resistances at the first 136 h, and the HSLA steel presents improved corrosion resistance in the final experiment. The corrosion process is greatly influenced by the gain

size of the steel, the shape of Fe_3C in microstructure, and the deposition of $FeSO_4$ on the electrode surface.

References

1. Li DG, Feng YR, Bai ZM et al (2007) Electrochim Acta 52:7877. doi:10.1016/j.electacta.2007.06.059
2. Choi YS, Shim JJ, Kim JG (2004) Mater Sci Eng A 385:148
3. Choi YS, Kim JG (2000) Corrosion 56:1202
4. Alves VA, Bret CMA (2002) Electrochim Acta 47:2081. doi:10.1016/S0013-4686(02) 00077-4
5. Yang Q, Luo JL (2000) Electrochim Acta 45:3927. doi:10.1016/S0013-4686(00) 00492-8
6. Martini EMA, Muller IL (2000) Corros Sci 42:443. doi:10.1016/S0010-938X(99) 00064-5
7. Davies DH, Burstein GT (1980) Corrosion 36:416
8. Chinese Railway Standard Testing method for corrosivity of industrial gas, TBT2375, 1994, pp 1–6.
9. Meng GZ, Li Y, Wang FH (2006) Electrochim Acta 51:4277. doi:10.1016/j.electacta.2005.12.015
10. Christiansen KA, Hoeg H, Michelsen K et al (1961) Acta Chem Scand 15:300. doi:10.3891/acta.chem.scand.15-0300
11. Bockris JOM, Drazic D, Despic R (1961) Electrochim Acta 4:325. doi:10.1016/0013-4686(61) 80026-1
12. Albarran JL, Martinez L, Lopez HF (1999) Corros Sci 41:1049. doi:10.1016/S0010-938X(98) 00139-5
13. Wallinder D, Pan J, Lergraf C et al (1999) Corros Sci 41:275. doi:10.1016/S0010-938X(98) 00122-X
14. Dugstad A, Hemmer H, Seiersten M (2000) Proceeding of NACA Corrosion NACE 2000, Orlando, p 30
15. Tan YJ, Bailey S, Kinsella B (1996) Corros Sci 38:1545. doi:10.1016/0010-938X(96) 00047-9
16. Cao CN, Zhang JQ (2002) An introduction to electrochemical impedance spectroscopy. Science, Beijing, China
17. Wallinder D, Pan J, Lergraf C (1999) Corros Sci 41:275. doi:10.1016/S0010-938X(98) 00122-X
18. Macák J, Sajdl P, Kučera P (2006) Electrochim Acta 51:3573. doi:10.1016/j.electacta.2005.10.013
19. Zhang CL, Cai DY, Liao B (2004) Mater Lett 58:1524. doi:10.1016/j.matlet.2003.10.018
20. Vera R, Rosales BM, Tapia C (2003) Corros Sci 45:321. doi:10.1016/S0010-938X(02) 00071-9
21. Li DY (2006) Mater Rec Soc Symp Proc 887:227
22. Li W, Li DY (2005) Appl Surf Sci 240:388. doi:10.1016/j.apsusc.2004.07.017
23. Mora-Mendoza JL, Turgoose S (2002) Corros Sci 44:1223. doi:10.1016/S0010-938X(01) 00141-X
24. Malik H (1995) Corrosion 51:321